

AAK24: Global QCD analysis on polarized parton distribution in the presence of A_2 asymmetry measurements

Fatemeh Arbabifar^{1a}, Shahin Atashbar Tehrani^{2,3b}, and Hamzeh Khanpour^{4,2,5c}

¹ Department of Physics Education, Farhangian University, P.O.Box 14665-889, Tehran, Iran.

² School of Particles and Accelerators, Institute for Research in Fundamental Sciences (IPM), P.O.Box 19395-5531, Tehran, Iran

³ Department of Physics, Faculty of Nano and Bio Science and Technology, Persian Gulf University, 75169 Bushehr, Iran.

⁴ AGH University, Faculty of Physics and Applied Computer Science, Al. Mickiewicza 30, 30-055 Kraków, Poland.

⁵ Department of Physics, University of Science and Technology of Mazandaran, P.O.Box 48518-78195, Behshahr, Iran.

Received: April 25, 2024 / Revised version: August 30, 2024

Abstract. This article introduces AAK24, a Next-to-Leading Order (NLO) QCD analysis of polarized data from both polarized Deep Inelastic Scattering (DIS) and Semi-Inclusive Deep Inelastic Scattering (SIDIS) experiments on the nucleon. The AAK24 QCD analysis incorporates SU(2) and SU(3) symmetry breaking, specifically $\delta\bar{u} \neq \delta\bar{d} \neq \delta\bar{s}$, while assuming $\delta\bar{s}$ and δs are equal. Emphasizing the significance of the semi-inclusive data, the study explores the determination of polarized sea quark distributions. Recent experimental data from JLAB17, COMPASS16, and COMPASS17, including the A_2 asymmetry measurements along with SIDIS observables, are thoroughly examined for their impact on the central values of polarized PDFs, their uncertainties, and overall fit quality. Additionally, we include the nonperturbative target mass corrections (TMC) as well as higher-twist terms (HT) which are particularly important. In this work, the uncertainties are quantified using the standard Hessian method. The main results and findings of the AAK24 QCD analysis show overall good agreement with the analyzed experimental data, aligning well with other polarized PDF determinations, particularly DSSV14, LSS10, JAM17, and AKS14, all considering SU(2) and SU(3) symmetry breaking.

1 Introduction

In recent years, advancements in the determination of the nucleon partonic distributions and spin projections, particularly from high-energy experimental data, have significantly enhanced our understanding in this area [1, 2, 3, 4, 5, 6]. Extracting the polarized and unpolarized partonic distributions from QCD analysis is pivotal for studying the phenomenology of hard scattering processes [2]. The determination of polarized parton distribution functions (polarized PDFs) and along their uncertainties has rapidly expanded, driven by polarized deep inelastic scattering (DIS) experiments at CERN, SLAC, DESY, and JLAB [7, 8, 9, 20, 10, 11, 12, 16, 24, 13, 17], along with the inclusion of semi-inclusive deep inelastic scattering (SIDIS) data by various phenomenological groups [18, 22, 19, 23].

In this work, we utilize comprehensive proton and deuteron SIDIS asymmetry data sets from SMC and COMPASS group at CERN, including the semi-inclusive asymmetries for charged pion (π^\pm), kaon (k^\pm) and light charged hadron (h^\pm) production from a polarized proton target. Using the SIDIS asymmetry data sets, we take into account the flavor SU(2) and SU(3) symmetry breaking as well. The recent experimental data from JLAB17 [28], COMPASS16 [27], and COMPASS17 [6] experiments have been incorporated into our data samples. More importantly, this analysis marks the first simultaneous incorporation of SIDIS data and the A_2 asymmetry measurements for proton, neutron and deuteron from SLAC/E143, SMC, HERMES, and Jlab-Hall A experiments as well. We have thoroughly examined the impact of these new data sets on both the central values and extracted uncertainties, as well as their effect on the overall fit quality. Additionally, we calculate the uncertainty of polarized PDFs using the standard Hessian method.

This paper is organized as follows: Sec. 2 outlines the basic theoretical formalism utilized in the analysis of polarized PDFs within the context of AAK24. Sec. 3 discusses the details of the polarized DIS and SIDIS datasets for proton,

^a F.Arbabifar@cfu.ac.ir

^b Atashbar@ipm.ir

^c Hamzeh.Khanpour@cern.ch

neutron, and deuteron targets. In Sec. 4, we present and discuss the AAK24 parametrization of polarized PDFs and the assumptions that have considered. Sec. 5 introduces the AAK24 methodology employed for extracting the polarized PDFs, the fitting procedure, and estimating their uncertainties, specifically through the standard Hessian method. Sec. 6 presents the full results and findings of this work, comparisons with other models, and discussion of data/theory agreement as well. We also discuss the effects arising from the inclusion of the new data sets added to this analysis. Finally, Sec. 7 provides a comprehensive summary and conclusion of the work.

2 Theoretical framework

In the following, we present a brief review of the basic theoretical formalism employed in the analysis of polarized PDFs within the context of AAK24. Our discussion in this section primarily focuses on two key aspects: the spin-dependent structure function within the framework of QCD, and the unpolarized structure function as well. The inclusion of the unpolarized structure function is essential as it plays a pivotal role in extracting the polarized PDFs from the measured asymmetries. Furthermore, we also present and discuss the observables used in this work to extract the AAK24 polarized PDFs.

In perturbative QCD, the spin structure function g_1 for $Q^2 \gg \Lambda^2$ (without specifying the nucleon target label N) can be expressed as:

$$g_1(x, Q^2) = g_1^{\tau 2 + \text{TMCs}}(x, Q^2) + g_1(x, Q^2)_{\text{HT}} , \quad (1)$$

In this equation, $g_1^{\tau 2 + \text{TMCs}}(x, Q^2)$ represents the leading twist ($\tau = 2$) contribution to the g_1 structure function, including the effects of target mass corrections (TMCs). The term $g_1(x, Q^2)_{\text{HT}}$ accounts for the contributions from higher-twist QCD operators as well.

The $g_1(x, Q^2)^{\tau 2}$ is the well-known (logarithmic in Q^2) NLO perturbative QCD contribution, and can be written as,

$$g_1(x, Q^2)^{\tau 2} = \frac{1}{2} \sum_{q, \bar{q}}^{n_f} e_q^2 \left\{ \left[1 + \frac{\alpha_s}{2\pi} \delta C_q \right] \otimes \delta q(x, Q^2) + \frac{\alpha_s}{2\pi} 2\delta C_g \otimes \delta g(x, Q^2) \right\} . \quad (2)$$

In equation above, α_s represents the strong coupling constant at NLO accuracy, and δq , $\delta \bar{q}$, and δg correspond to the polarized quark, antiquark, and gluon density functions, respectively. In Eq. 2, the symbol \otimes represents the convolution integral. The terms δC_q and δC_g denote the corresponding hard scattering Wilson coefficients, which are calculable in perturbative QCD and can be found, for example, in Refs. [29,19]. The explicit twist-2 expression for the g_1 in the presence of TMCs can be written as [30,31,32,33,34]:

$$\begin{aligned} & g_1^{\tau 2 + \text{TMCs}}(x, Q^2) \\ &= \frac{x g_1^{\tau 2}(\xi, Q^2; M=0)}{\xi(1 + 4M^2 x^2/Q^2)^{3/2}} + \frac{4M^2 x^2}{Q^2} \frac{(x + \xi)}{\xi(1 + 4M^2 x^2/Q^2)^2} \int_{\xi}^1 \frac{d\xi'}{\xi'} g_1^{\tau 2}(\xi', Q^2; M=0) \\ & - \frac{4M^2 x^2}{Q^2} \frac{(2 - 4M^2 x^2/Q^2)}{2(1 + 4M^2 x^2/Q^2)^{5/2}} \times \int_{\xi}^1 \frac{d\xi'}{\xi'} \int_{\xi'}^1 \frac{d\xi''}{\xi''} g_1^{\tau 2}(\xi'', Q^2; M=0) , \end{aligned} \quad (3)$$

in which, M denotes the nucleon mass. The parameter ξ in the above equation refers to the Nachtmann variable [35], which is defined as:

$$\xi = \frac{2x}{1 + \sqrt{1 + 4M^2 x^2/Q^2}} . \quad (4)$$

The maximum kinematic value of the Nachtmann variable ξ presented above is less than unity, implying that both the polarized and unpolarized target mass-corrected leading-twist structure functions do not vanish at $x = 1$. Finally, the dynamical higher-twist effects are given by:

$$g_1(x, Q^2)_{\text{HT}} = \frac{h(x, Q^2)}{Q^2} + \mathcal{O}\left(\frac{\Lambda^4}{Q^4}\right) . \quad (5)$$

This contribution is fitted to the data along with the fit parameters.

Given that AAK24 is limited to the NLO accuracy, consistent with most global polarized PDF analyses available in literature, we utilize the hard scattering coefficients computed to the same NLO order. In addition, n_f is the number of active flavors ($n_f = 3$ in our analysis).

In the leading-twist approximation and at the NLO accuracy, the $g_2(x, Q^2)$ spin-dependent structure-function which contains the transverse spin carried by the nucleons is given in terms of the twist-2 component of $g_1(x, Q^2)$ via the Wandzura-Wilczek relation, as detailed in Refs. [36]. The $g_2(x, Q^2)$ can be written as,

$$g_2(x, Q^2) = -g_1(x, Q^2) + \int_x^1 \frac{dy}{y} g_1(y, Q^2). \quad (6)$$

It is important to note that these leading-twist approximation results are, strictly speaking, valid in the Bjorken limit $Q^2 \rightarrow \infty$ for a given fixed value of x . At the finite values of photon virtuality Q^2 the power-suppressed corrections to the spin-dependent structure function can make important contributions, particularly in specific kinematic regions. The simplest of these are the target mass corrections (TMCs) in which studied in details in our prior analysis [20], and it has also been examined in other studies found in the literature, such as [24, 37, 38]. In the following analysis, we consider the TMC and HT corrections as presented in Eqs. 3 and 5.

The unpolarized structure function $F_1(x, Q^2)$, which is essential for extracting the polarized PDFs from the measured asymmetries, can be expressed as follows:

$$F_1(x, Q^2) = \frac{(1 + \gamma^2)}{2x(1 + R(x, Q^2))} F_2(x, Q^2), \quad (7)$$

in which is determined per kinetic variables x , R and the nucleon unpolarized structure function $F_2(x, Q^2)$. In Eq. 7, the factor γ^2 defined as $\frac{4M^2 x^2}{Q^2}$, and R is the ratio of the longitudinal σ_L to the transverse σ_T virtual photoproduction cross sections; $R = \frac{\sigma_L}{\sigma_T}$ [39], which in our calculations, we use the experimental values measurement by NMC collaboration [40].

The virtual photoproduction longitudinal and transverse asymmetries in the Bjorken limit can be expressed as ratios of the spin-dependent ($g_1(x, Q^2)$ and $g_2(x, Q^2)$) and unpolarized ($F_1(x, Q^2)$ and $F_2(x, Q^2)$) structure functions.

Finally, having at hand the spin-dependent and unpolarized structure functions, one can define the A_1 and A_2 asymmetries for polarized DIS processes as follows:

$$A_1(x, Q^2) = \frac{g_1(x, Q^2)}{F_1(x, Q^2)} (1 + \gamma^2), \quad (8)$$

for A_1 , and

$$A_2(x, Q^2) = \gamma \frac{g_1(x, Q^2) + g_2(x, Q^2)}{F_1(x, Q^2)}, \quad (9)$$

for the A_2 asymmetries, respectively.

We should stress here that, a very large data sample of the A_2 asymmetry has been incorporated into the AAK24 QCD analysis. We will provide a comprehensive discussion of this dataset in the forthcoming section. The effect of the A_2 asymmetry data on the extracted polarized PDFs are studied and clearly discussed in Sec. 6 as well.

As previously emphasized, one of the primary objectives of this study is to incorporate the SIDIS data alongside the polarized DIS data, thereby enabling the examination of light sea-quark decomposition and to provide well-constrained gluon PDFs. In order to increase the statistics of the SIDIS observables, we utilize the most recent and precise experimental data measured by JLAB17, COMPASS16, and COMPASS17 experiments.

At the leading-twist approximation and at NLO accuracy, the spin-dependent structure function $g_{1N}^h(x, z, Q^2)$ for the SIDIS processes can be calculated in terms of the polarized PDFs and the Fragmentation Function (FFs). It reads,

$$g_{1N}^{h, twist-2}(x, z, Q^2) = \frac{1}{2} \sum_{q, \bar{q}}^{n_f} e_q^2 \left\{ \left[\delta q \left(1 + \otimes \frac{\alpha_s(Q^2)}{2\pi} \delta C_{qq} \otimes \right) D_q^h + \delta q \otimes \frac{\alpha_s(Q^2)}{2\pi} \delta C_{gq}^{(1)} \otimes D_g^h + \delta g \otimes \frac{\alpha_s(Q^2)}{2\pi} \delta C_{qg}^{(1)} \otimes D_q^h \right] (x, z, Q^2) \right\}, \quad (10)$$

in which the δq , $\delta \bar{q}$ and δg are the polarized quark, antiquark and gluon density functions, the C_{qq} , C_{qg} and C_{gg} denote the corresponding hard scattering Wilson coefficients. The D_q^h and D_g^h are the corresponding FFs of a given hadron.

The unpolarized structure function of $F_{1N}^h(x, z, Q^2)$ for a SIDIS process is given by,

$$F_{1N}^{h,twist-2}(x, z, Q^2) = \frac{1}{2} \sum_{q, \bar{q}}^{n_f} e_q^2 \left\{ \left[q \left(1 + \frac{\alpha_s(Q^2)}{2\pi} C_{qq} \otimes \right) D_q^h + q \otimes \frac{\alpha_s(Q^2)}{2\pi} C_{gq}^{(1)} \otimes D_g^h + g \otimes \frac{\alpha_s(Q^2)}{2\pi} C_{gg}^{(1)} \otimes D_g^h \right] (x, z, Q^2) \right\} \quad (11)$$

where the q and g are the unpolarized PDFs, the D_q^h and D_g^h are the quark and gluon FFs of hadron. Finally, the $C_{q(g)g(q)}$ are the hard scattering Wilson coefficients available in literature [41, 19]. In the following analysis, we use the publicly available unpolarized PDFs of CT18 group [43] and for the quark and gluon FFs of hadron we employ the DSS [44] results.

The observable for the SIDIS process that we used in AAK24 QCD analysis is the A_{1N}^h asymmetry which can be calculated as ratio of spin-dependent structure function $g_{1N}^h(x, z, Q^2)$ and $g_{2N}^h(x, z, Q^2)$ to the unpolarized structure function $F_{1N}^h(x, z, Q^2)$. It is given by [23],

$$A_{1N}^h(x, z, Q^2) = \frac{g_{1N}^h(x, z, Q^2) - \gamma^2 g_{2N}^h(x, z, Q^2)}{F_{1N}^h(x, z, Q^2)}, \quad (12)$$

As in the case of polarized DIS, the factor γ^2 is defined as $\frac{4M^2 x^2}{Q^2}$. In this work, we do not include HT and TMC corrections for the case of SIDIS observables. The HT and TMC corrections are expected to be less significant due to the kinematic region and the precision of the currently available SIDIS data sets [23].

Having defined the polarized observables $A_1(x, Q^2)$, $A_2(x, Q^2)$, $A_{1N}^h(x, z, Q^2)$ and the structure functions necessary for the AAK24 QCD-based analysis, our next step in the upcoming section is to present an overview of the polarized inclusive DIS and SIDIS datasets that are subject to analysis in this study.

3 Polarized inclusive DIS and SIDIS datasets

As we discussed earlier, in AAK24 QCD analysis, we use two types of datasets from polarized DIS and SIDIS experiments on proton, neutron and deuteron targets which mostly come from relevant experiments that were done at DESY, SLAC, JLAB and CERN. Our objective is to comprehensively incorporate all available data from polarized DIS and SIDIS experiments, ensuring coverage across a wide range of kinematic variables in terms of both x and Q^2 . In the following, we will discuss in details the datasets analyzed in our work.

From a statistical perspective, the wealth of experimental datasets used in our analysis are for the inclusive polarized DIS experiments for A_1 asymmetry for lepton scattering from stationary targets with various combinations of targets and lepton spin.

The published experimental datasets for the A_1 and $\frac{g_1}{F_1}$ observables are comprehensively presented in Table. 1. This table provides details on the measured observables, their kinematic coverage in terms of x and Q^2 , as well as references to the publications where these datasets can be found.

These datasets have been measured and published by various experimental collaborations, including COMPASS [6, 27, 47], JLAB [28, 57], CLAS [56], EMC [45], SMC [46], SLAC [48, 49, 50, 51, 52], and HERMES [54, 55].

It is worth noting that, in AAK24 QCD analysis, we have analyzed the latest A_1 asymmetry data from the COMPASS experiment at CERN, encompassing measurements on proton, neutron, and deuteron targets, COMPASS16 [6] and COMPASS17 [27]. For the case of COMPASS16 in which cover the range from 1 to 190 GeV² in the photon virtuality and from 0.0025 to 0.7 in the Bjorken scaling variable x , they improved the statistical precision of g_1^p by about a factor of two in the newly explored low- x region $x < 0.02$.

The COMPASS17 data were taken at 160 GeV² beam energy and the results are presented for the kinematic range 1 to 100 GeV² in photon virtuality, and $4 \times 10^{-3} < x < 0.7$ in the Bjorken scaling variable, and $W > 4$ GeV² in the mass of the hadronic final state.

As indicated in Table. 1, the recently incorporated data from the COMPASS experiment are particularly valuable as they offer measurements at the lowest accessible values of x , (approximately $x \sim 4 \times 10^{-3}$). Consequently, these data play a crucial role in accurately determining the polarization information of gluons and sea quarks through inclusive polarized DIS data analysis.

In addition to the COMPASS data, we have incorporated the recent A_1 asymmetry data from the JLAB experiment, focusing on measurements with the proton target, as detailed in Ref. [28]. This inclusion further enriches our dataset for analysis.

The CLAS experiment [56], contributes significantly to our dataset, providing nearly 60 percent of the total data points. In total, we include 996 data points for the A_1 and $\frac{g_1}{F_1}$ asymmetry measurements. The E155 [51,52], HERMES [54] and JLAB [57] experiment present special cases of g_1/F_1 .

Experiment	Process	N_{data}	x_{min}	x_{max}	$Q_{\text{min}}^2 [\text{GeV}^2]$	$Q_{\text{max}}^2 [\text{GeV}^2]$	Observable	χ^2	χ^2 (Exc. A_2)
COMPASS16 [6]	DIS(p)	44	0.0045	0.58	1.02	82.04	A_1^p	40.188	39.361
COMPASS17 [27]	DIS(d)	43	0.0045	0.569	1.03	74.1	A_1^d	34.269	33.737
JLAB17 [28]	DIS(p)	10	0.15733	0.58355	1.0522	4.1293	A_1^p	36.312	36.478
EMC [45]	DIS(p)	10	0.015	0.466	3.5	29.5	A_1^p	4.100	4.686
SMC [46]	DIS(p)	12	0.005	0.48	1.3	58	A_1^p	4.315	4.526
SMC [46]	DIS(d)	12	0.005	0.479	1.3	54.8	A_1^d	21.428	21.261
COMPASS [47]	DIS(p)	15	0.0046	0.568	1.1	62.1	A_1^p	11.601	11.186
SLAC/E142 [48]	DIS(n)	8	0.035	0.466	1.1	5.5	A_1^n	7.404	4.445
SLAC/E143 [49]	DIS(p)	28	0.031	0.749	1.27	9.52	A_1^p	21.111	20.757
SLAC/E143 [49]	DIS(d)	28	0.031	0.749	1.27	9.52	A_1^d	52.322	50.999
SLAC/E154 [50]	DIS(n)	11	0.017	0.564	1.2	15	A_1^n	3.805	3.803
SLAC/E155 [51]	DIS(p)	24	0.015	0.75	1.22	34.72	$\frac{g_1^p}{F_1^p}$	29.226	34.812
SLAC/E155 [52]	DIS(d)	24	0.015	0.75	1.22	34.72	$\frac{g_1^d}{F_1^d}$	21.652	21.450
HERMES [54]	DIS(n)	9	0.033	0.464	1.22	5.25	A_1^n	3.939	3.460
HERMES [54]	DIS(p)	19	0.028	0.66	1.01	7.36	$\frac{g_1^p}{F_1^p}$	16.324	16.092
HERMES [55]	DIS(p)	15	0.0264	0.7248	1.12	12.21	A_1^p	10.284	9.947
HERMES [55]	DIS(d)	15	0.0264	0.7248	1.12	12.21	A_1^d	19.408	19.569
JLab-Hall A [57]	DIS(n)	3	0.33	0.6	2.71	4.38	$\frac{g_1^n}{F_1^n}$	2.396	1.840
CLAS [56]	DIS(p)	151	0.1088	0.5916	1.01	4.96	A_1^p	140.949	145.795
CLAS [56]	DIS(d)	482	0.1366	0.57	1.01	4.16	A_1^d	434.995	441.439
TOTAL:		951						916.038	925.652

Table 1. The published experimental data sets for A_1^N and $\frac{g_1^N}{F_1^N}$ asymmetry measurements from different experiments for different polarized DIS target. The measured observables, their kinematic range in x and Q^2 , and the published references are also shown. The individual χ^2 values per data point for both the analysis with and without A_2 asymmetry data are also presented. The details of the kinematical cuts applied on the data and the method on χ^2 minimization are explained in the text.

In Fig. 1, the kinematic coverage of the A_1^N asymmetry measurement dataset is represented in the x and Q^2 plane. The data points are categorized by different experiments, as illustrated in the presentation of the dataset. As one can see, the newly added data from COMPASS experiment offer measurements at the lowest accessible values of Bjorken variable x , ($x \sim 4 \times 10^{-3}$).

In the AAK24 global polarized PDF analysis, we incorporate, for the first time, all available worldwide data on the inclusive DIS of leptons on proton, neutron, and deuteron targets for the measurement of the A_2 asymmetry measurement. This comprehensive inclusion expect to enhance the coverage and precision of the analysis.

This inclusion encompasses all datasets from various experiments, including SLAC/E143 [58, 49, 59, 60, 61, 61], SMC [62], JLab-Hall A [57], as well as recent high-precision asymmetry measurements from HERMES [63]. The datasets for the A_2 asymmetry measurement are presented in detail in Table. 2. This table provides the kinematic coverage in terms of x and Q^2 , as well as references to the corresponding publications. The A_2^N asymmetry measurements include 140 data points. To assess the impact of these data sets, two distinct analyses were conducted in this work, with and without the inclusion of A_2^N asymmetry measurements. A detailed discussion on this matter is provided in Sec. 6.

In Fig. 2, the kinematic coverage of the A_2 asymmetry measurement are presented in the x and Q^2 plane. The data points are categorized by different experiments as well.

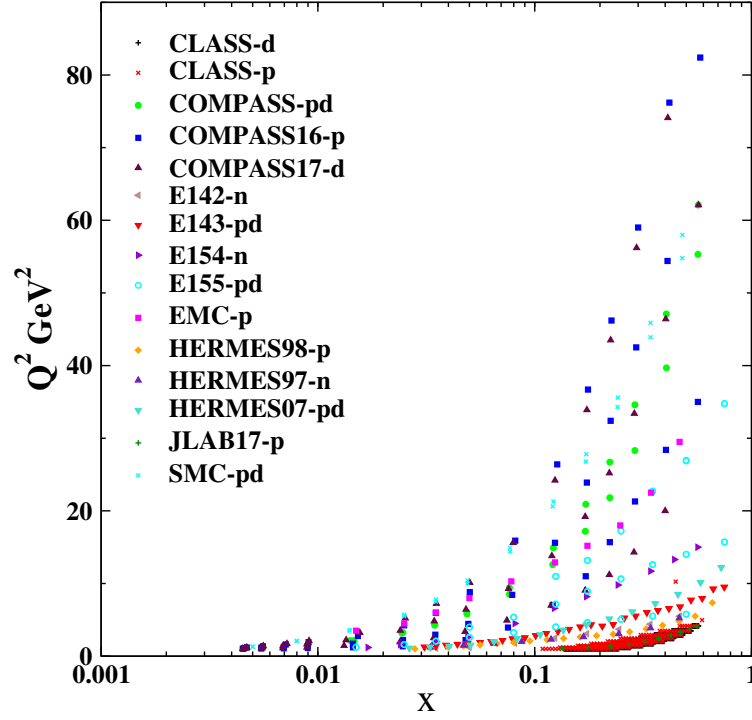


Fig. 1. The kinematic coverage in the x and Q^2 plane of the A_1^N asymmetry measurement data set. The data points are classified by different experiments.

Experiment	Process	N_{data}	x_{\min}	x_{\max}	Q_{\min}^2 [GeV ²]	Q_{\max}^2 [GeV ²]	Observable	χ^2
SLAC/E143 [58]	DIS(p)	12	0.038	0.595	1.49	8.85	A_2^p	7.260
SLAC/E143 [58]	DIS(d)	12	0.038	0.594	1.49	8.84	A_2^d	11.441
SLAC/E143 [49]	DIS(p)	12	0.038	0.595	1.49	8.85	A_2^p	7.414
SLAC/E143 [49]	DIS(d)	12	0.038	0.595	1.49	8.86	A_2^d	11.870
SLAC/E143 [49]	DIS(n)	12	0.038	0.595	1.49	8.86	A_2^n	7.414
SLAC/E155 [59]	DIS(p)	8	0.038	0.78	1.1	8.4	A_2^p	9.130
SLAC/E155 [59]	DIS(d)	8	0.038	0.78	1.1	8.4	A_2^d	14.759
SLAC/E155 [60]	DIS(p)	10	0.022	0.839	1.15	27.18	A_2^p	46.832
SLAC/E155 [60]	DIS(d)	10	0.022	0.839	1.15	27.18	A_2^d	21.102
SLAC/E154 [61]	DIS(n)	17	0.017	0.564	1.2	15	A_2^n	0.736
SMC [62]	DIS(d)	4	0.0108	0.228	2.6	18	A_2^d	6.224
HERMES [63]	DIS(p)	20	0.039	0.678	1.09	10.35	A_2^p	20.394
JLab-Hall A [57]	DIS(n)	3	0.33	0.6	2.71	4.38	A_2^n	3.369
TOTAL:		140						113.703

Table 2. Same as Table. 1 but this time for the A_2^N asymmetry measurement.

In our analysis, we have also incorporated all available data for the SIDIS process, covering various detected hadrons, including pions (π^\pm), kaons (k^\pm), and light-charged hadrons (h^\pm). This comprehensive addition further enhances the richness and diversity of our dataset for analysis. The published data points are related to the $A_1^{N,h}$ asymmetry, as described in Eq. 12, originating from the SIDIS processes. The SIDIS observables are instrumental in enabling the consideration of flavor decomposition within the sea-quark density. These observables provide valuable information about the different flavors of sea quarks within the nucleon.

The measurements of the $A_1^{N,h}$ asymmetry, encompassing data from various experiments, incorporate datasets from SMC [53], COMPASS08 [64], and COMPASS09 [65]. Furthermore, the recently obtained and highly precise proton data from the COMPASS10 experiment [66], have been included in our QCD analysis.

The analyzed SIDIS data have been comprehensively summarized in Table. 3. This table provides a classification of the data based on each experiment and different detected hadrons, which include pions (π^\pm) and kaons (k^\pm), and light-charged hadrons (h^\pm). In the AAK24 QCD fit, a total of 160 data points from the SIDIS process have been utilized.

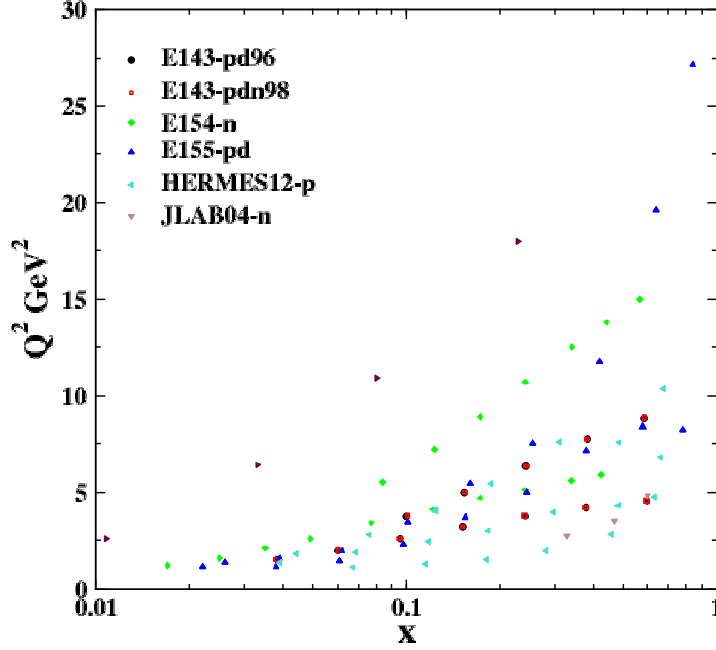


Fig. 2. The kinematic coverage in the x and Q^2 plane for the A_2^N asymmetry measurement in which, for the first time, analyzed in AAK24 QCD analysis. The data points are classified by different experiments.

The kinematic coverage of the $A_1^{N,h}$ asymmetry measurement are presented in Fig. 3 in the x and Q^2 plane. The data points are categorized by different experiments as well.

All the datasets analyzed in AAK24 polarized PDFs are subject to the cut on the $Q^2 \geq 1 \text{ GeV}^2$, in which below $Q^2 = 1 \text{ GeV}^2$ the perturbative QCD is not reliable. For all polarized DIS experiments where they are available, we fit directly the asymmetries of A_1 and A_2 .

4 AAK24 parametrization of polarized PDFs

In this section, we will present and discuss the AAK24 parametrization of polarized PDFs and the assumptions that we have considered. For the generic parametrization of polarized PDFs, assigned to each parton at a specified input scale of $Q_0^2 = 1 \text{ GeV}^2$, we choose the following standard functional form,

$$x \delta q = \mathcal{N}_q \eta_q x^{a_q} (1-x)^{b_q} (1 + c_q x^{0.5} + d_q x), \quad (13)$$

which is defined in terms of five shape fit parameters η_q , a_q , b_q , c_q and d_q , and the normalization factor \mathcal{N}_q as well. The normalization factor \mathcal{N} in Eq. 13 is calculated as follows:

$$\begin{aligned} \frac{1}{\mathcal{N}_q} = & \left(1 + d_q \frac{a_q}{a_q + b_q + 1} \right) B(a_q, b_q + 1) \\ & + c_q B\left(a_q + \frac{1}{2}, b_q + 1\right), \end{aligned} \quad (14)$$

Experiment	Process	N_{data}	x_{min}	x_{max}	Q_{min}^2 [GeV ²]	Q_{max}^2 [GeV ²]	Observable	χ^2	χ^2 (Exc. A_2)
SMC [53]	SIDIS(p, h^+)	12	0.005	0.48	10	10	A_1^{p,h^+}	24.973	26.246
SMC [53]	SIDIS(p, h^-)	12	0.005	0.48	10	10	A_1^{p,h^-}	12.096	12.497
SMC [53]	SIDIS(d, h^+)	12	0.005	0.48	10	10	A_1^{d,h^+}	6.131	6.514
SMC [53]	SIDIS(d, h^-)	12	0.005	0.48	10	10	A_1^{d,h^-}	16.697	17.004
COMPASS08 [64]	SIDIS(d, h^+)	12	0.0052	0.482	1.17	60.2	A_1^{d,h^+}	16.108	17.906
COMPASS08 [64]	SIDIS(d, h^-)	12	0.0052	0.482	1.17	60.2	A_1^{d,h^-}	18.210	18.178
COMPASS09 [65]	SIDIS(d, π^+)	10	0.0052	0.24	1.16	32.8	A_1^{d,π^+}	11.598	13.578
COMPASS09 [65]	SIDIS(d, π^-)	10	0.0052	0.24	1.16	32.8	A_1^{d,π^-}	13.476	12.296
COMPASS09 [65]	SIDIS(d, k^+)	10	0.0052	0.24	1.16	32.8	A_1^{d,k^+}	26.377	29.621
COMPASS09 [65]	SIDIS(d, k^-)	10	0.0052	0.24	1.16	32.8	A_1^{d,k^-}	26.354	29.791
COMPASS10 [66]	SIDIS(p, π^+)	12	0.0052	0.48	1.16	55.6	A_1^{p,π^+}	15.294	15.853
COMPASS10 [66]	SIDIS(p, π^-)	12	0.0052	0.48	1.16	55.6	A_1^{p,π^-}	13.491	15.303
COMPASS10 [66]	SIDIS(p, k^+)	12	0.0052	0.48	1.16	55.6	A_1^{p,k^+}	20.450	22.077
COMPASS10 [66]	SIDIS(p, k^-)	12	0.0052	0.48	1.16	55.6	A_1^{p,k^-}	6.673	7.648
TOTAL:		160						227.934	244.520

Table 3. The published data points for the $A_1^{N,h}$ asymmetry measured by SMC and COMPASS collaborations on different targets. The measured observables, the number of data points, their kinematic range in x and Q^2 , and the published references are also shown. The individual χ^2 values per data point for both the analysis with and without A_2 asymmetry data are also presented.

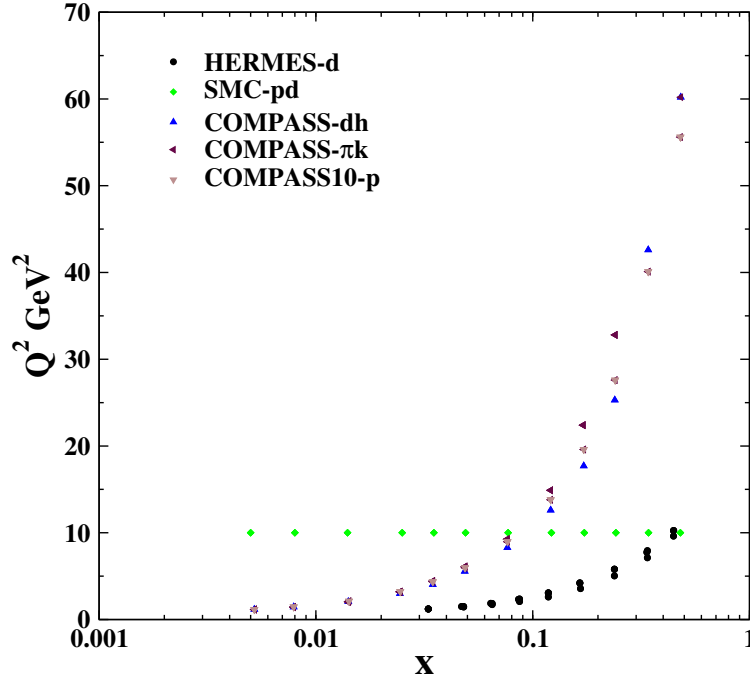


Fig. 3. The kinematic coverage in the x and Q^2 plane of the $A_1^{N,h}$ asymmetry measurement data set. The data points are classified by different experiments.

which is chosen such that the η_q represents the first moments of $\delta q(x, Q_0^2)$. The $B(a, b)$ indicates to the Euler beta function.

Since the AAK24 QCD analysis considers inclusive DIS data and the SIDIS observables as well, we attempt to consider the flavor asymmetric polarized PDFs and try to fit the PDFs $\delta q = \delta u + \delta \bar{u}, \delta d + \delta \bar{d}, \delta \bar{u}, \delta \bar{d}, \delta \bar{s}$ and δg at the input scale.

The observables obtained from the SIDIS processes can, in principle, provide the capability to distinguish between the strange quark density (δs) and its antiquark counterpart ($\delta \bar{s}$) through separate production of K^+ and K^- mesons.

However, in practice, our current fit lacks the sensitivity to achieve a clear separation between these distributions. Therefore, in line with the polarized PDF analyses conducted in Refs. [24,19], we make the assumption of a flavor-symmetric strange quark distribution, meaning that $\delta s(x, Q^2) = \delta \bar{s}(x, Q^2)$. To control the behavior of $\delta \bar{u}$ and $\delta \bar{d}$ distributions over the small x region, additional constraints on the shape parameters are applied by assuming $a_{\delta u + \delta \bar{u}} = a_{\delta \bar{u}}$, and $a_{\delta d + \delta \bar{d}} = a_{\delta \bar{d}} = a_{\delta s}$ as well.

In general, polarized PDF analyses utilize two well-known sum rules that relate the first moments of polarized PDFs to the F and D quantities, which are evaluated in neutron and hyperon β -decays [25] under the assumption of SU(2) and SU(3) flavor symmetries:

$$a_3 = \Delta \Sigma_u - \Delta \Sigma_d = F + D, \quad (15)$$

$$a_8 = \Delta \Sigma_u + \Delta \Sigma_d - 2\Delta \Sigma_s = 3F - D. \quad (16)$$

Here, a_3 and a_8 represent non-singlet combinations of the first moments of the polarized parton distributions, corresponding to the non-singlet q_3 and q_8 distributions:

$$q_3 = (\delta u + \delta \bar{u}) - (\delta d + \delta \bar{d}), \quad (17)$$

$$q_8 = (\delta u + \delta \bar{u}) + (\delta d + \delta \bar{d}) - 2(\delta s + \delta \bar{s}). \quad (18)$$

A recent reanalysis of the F and D parameters, with updated β -decay constants [25], yielded $F = 0.464 \pm 0.008$ and $D = 0.806 \pm 0.008$. We have utilized these updated values in our current analysis. However, since our focus is not on flavor symmetry and we have $\delta \bar{u} \neq \delta \bar{d} \neq \delta s$, we can use the combination of Eqs. 15 and 16 as follows:

$$\begin{aligned} \Delta u + \Delta \bar{u} &= 0.9275 + \Delta s + \Delta \bar{s}, \\ \Delta d + \Delta \bar{d} &= -0.3415 + \Delta s + \Delta \bar{s}. \end{aligned} \quad (19)$$

We apply these relations in our analysis, thus excluding the parameters that define the first moments of $(\delta u + \delta \bar{u})$ and $(\delta d + \delta \bar{d})$ (i.e., $\eta_{u+\bar{u}}$ and $\eta_{d+\bar{d}}$) from the analysis and obtaining them using Eq. 19. The impact of symmetry breaking on the first moments of polarized PDFs has been discussed in detail in the literature [26,17].

It is important to mention that the calculations take into account Isospin symmetry for both the proton and neutron. This symmetry is defined as follows:

$$\begin{aligned} \delta u^p &= \delta d^n ; \delta \bar{u}^p = \delta \bar{d}^n ; \delta d^p = \delta u^n \\ \delta \bar{d}^p &= \delta \bar{u}^n ; \delta s^p = \delta s^n ; \delta \bar{s}^p = \delta \bar{s}^n. \end{aligned} \quad (20)$$

Finally, we should highlight here that for some shape parameters as presented in Eq. 13 may lack strong constraints from available data. In such cases, additional assumptions become necessary. We will provide a detailed discussion of these assumptions, as considered in the AAK24 analysis, in Sec. 6.1.

5 Minimization strategy

In this section, we will introduce the AAK24 methodology employed for extracting polarized PDFs and for estimating their uncertainties, specifically through the standard Hessian method.

The AAK24 best-fit parameters are determined through the minimization of the χ^2 function, which is defined as follows:

$$\begin{aligned} \chi_{\text{global}}^2 &= \sum_n w_n \chi_n^2, \\ \chi_n^2 &= \left(\frac{1 - N_n}{\Delta N_n} \right)^2 + \sum_i \left(\frac{N_n A_{1,2,i}^{\text{data}} - A_{1,2,i}^{\text{theory}}}{N_n \Delta A_{1,2,i}^{\text{data}}} \right)^2, \end{aligned} \quad (21)$$

In the equation above, the quantity $A_{1,2,i}^{\text{data}}$ represents the measured value of the observable for the data point i from the experimental data set n . $A_{1,2,i}^{\text{theory}}$ refers to the corresponding theoretical value for the i^{th} experimental data point,

and $\Delta A_{1,2,i}^{\text{data}}$ denotes the experimental uncertainty, which is typically the combination of statistical and systematic uncertainties computed in quadrature. N_n is an overall normalization factor for the data of experimental data set n , and the ΔN_n is the experimental normalization uncertainty. We allow for a relative normalization shift N_n between different experimental data sets within uncertainties of ΔN_n quoted by the experiments.

For conducting the fitting process and deriving the AAK24 best-fit parameters, we utilize the publicly available MINUIT package, which has been developed by CERN [67]. A very good total $\chi^2/d.o.f = 1.0528$ value is achieved in these calculations. Table. 4 presents the numeric values of the AAK24 fit parameters obtained through the QCD analysis. The χ^2 values for the total and individual data sets are presented in Tables. 1, 2 and 3 respectively. The detailed discussions on the obtained best fit parameters, and the fit quality will be presented in Sec. 6.1.

At this point, we are ready to introduce the Hessian method for the estimation of polarized PDF uncertainty. The standard Hessian method employed in the AAK24 QCD analysis was originally developed in Refs. [42,68]. This method essentially aims to approximate the posterior distribution as a Gaussian distribution within the parameter space. To do this end, one first needs to find the set of parameters \mathbf{a}_0 corresponding to the maximum a posteriori estimate. These the set of parameters could be obtained by minimizing a certain the χ^2 function in Eq. 21. In a neighborhood of \mathbf{a}_0 parameters, the $\chi^2(\mathbf{a})$ function can be expanded up to the quadratic term in its parameters and the posterior approximated by a multi-dimensional Gaussian function,

$$p(\mathbf{a}|\mathbf{m}) \propto \exp\left(-\frac{1}{2}\chi^2(\mathbf{a}, m)\right) \propto \exp\left(-\frac{1}{2}\Delta\mathbf{a}^T H \Delta\mathbf{a}\right). \quad (22)$$

In the last term, $\Delta\mathbf{a} = \mathbf{a} - \mathbf{a}_0$, the Hessian matrix elements are given by

$$H_{ij} = \frac{1}{2} \left. \frac{\partial^2 \chi^2(\mathbf{a})}{\partial a^i \partial a^j} \right|_{\mathbf{a}=\mathbf{a}_0}, \quad i, j = 1, \dots, n_{\text{par}}. \quad (23)$$

and $\exp(-\frac{1}{2}\chi^2(\mathbf{a}_0))$ has been absorbed into the normalization of the posterior.

Additionally, the tolerances can be fine-tuned by setting a criterion that the χ^2 must increase above its minimum by a specified $\Delta\chi^2$ value, as discussed in Ref. [69]. In the AAK24 QCD analysis, fits will be conducted on a statistically consistent set of polarized DIS data, and thus, there is no need to employ a tolerance criterion. Nevertheless, it is important to calculate the tolerance explicitly in order to account for any actual deviations from Gaussian behavior and to obtain precise estimates of the variance. In the results that will be presented in the following Sec. 6, we take the tolerance criterion into account by setting $\Delta\chi^2 = T = 1$.

6 AAK24 fit results

This section includes the main results and findings of AAK24 polarized PDFs obtained from QCD analysis of polarized DIS and SIDIS data. We first present the AAK24 polarized PDFs, the fit parameters, and the results for different Parton species. Then we compare the AAK24 NLO theoretical predictions with the analyzed data. We also compare our results with other polarized PDFs available in the literature by discussing in detail the similarity and differences between these different polarized PDF sets.

6.1 AAK24 polarized PDFs

This section presents the AAK24 polarized PDFs at the input scale, the extracted best-fit parameters, and assumptions considered for the shape fit parameter as well.

The best fit parameters for AAK24 are presented in Table. 4. Upon examining the numbers presented in this table, several remarks are pertinent. In general, a QCD analysis of polarized DIS experiments should incorporate additional constraints on the shape parameters. This necessity arises from the affects of available data to fully constrain all parameters and the limited kinematic coverage of the data. Given that the existing experimental data sets lack the power to comprehensively determine the behavior of polarized PDFs, certain assumptions must be taken into consideration.

Firstly, to control the small x behavior of the $x\delta\bar{u}$, $x\delta\bar{d}$ and $x\delta s = x\delta\bar{s}$, we assume $a_{\delta u+\delta\bar{u}} = a_{\delta\bar{u}}$ and $a_{\delta d+\delta\bar{d}} = a_{\delta\bar{d}} = a_{\delta\bar{s}}$. Since we have determined that the best-fitted values of $b_{\delta\bar{u}}$, $b_{\delta\bar{d}}$, and $b_{\delta s=\delta\bar{s}}$ are not strongly constrained by the QCD fit and are very similar, all approximately equal to 10, we have chosen to maintain them as fixed values at 10.

Furthermore, we have observed that the parameter c_q for certain parton species, such as $x\delta u + x\delta\bar{u}$, $x\delta d + x\delta\bar{d}$, $x\delta\bar{s}$, and $x\delta g$, is extremely close to zero. As a result, we have opted to set these parameters to a fixed value of 0. Additionally, it is worth noting that some of the c and d shape parameters for the $x\delta\bar{d}$ density have been determined with relatively large errors. Incorporating additional high-energy polarized data sets from various types of experiments has the potential to alleviate some of the extra assumptions we have made regarding the shape parameters of the polarized distribution. To be more specific, the inclusion of proton-proton collision data from RHIC can have a significant impact on our understanding of the distributions within the nucleon, particularly in relation to the gluon PDFs.

Flavor	η_q	a_q	b_q	c_q	d_q
$\delta u + \delta\bar{u}$	0.863	0.4126 ± 0.0079	2.4636 ± 0.0174	0.0*	40.9115 ± 1.38
$\delta d + \delta\bar{d}$	-0.4053	0.2487 ± 0.0059	4.5203 ± 0.00272	0.0*	100.9866 ± 10.92
$\delta\bar{u}$	0.0639 ± 0.175	0.4126 ± 0.0079	10.0*	12.5012 ± 0.923	-39.5083 ± 8.09
$\delta\bar{d}$	-0.0288 ± 0.355	0.2487 ± 0.0059	10.0*	102.436 ± 52.07	800.569 ± 284.799
$\delta\bar{s}$	-0.0433 ± 0.0017	0.2487 ± 0.0059	10.0*	0.0*	-28.8485 ± 0.0027
δg	-0.3788 ± 0.0026	2.9019 ± 0.0908	10.0*	0.0*	-3.271 ± 0.0875

Table 4. The best-fitted values and their associated statistical errors are provided at the input scale $Q_0^2 = 1 \text{ GeV}^2$. It is important to note that parameters marked with an asterisk (*) have been held fixed.

As mentioned earlier, we also take into account the TMC and HT corrections, which play important roles in certain kinematic regions of x and Q^2 . The values of the HT corrections extracted from the data in our analysis are presented in Table. 5.

In Fig. 4, we display the AAK24 polarized PDFs at the input scale for all parton species including $x\delta u + x\delta\bar{u}$, $x\delta d + x\delta\bar{d}$, $x\delta\bar{u}$, $x\delta\bar{d}$, $x\delta\bar{s}$ and $x\delta g$. The results for the case where we have excluded the measurements of A_2^p , A_2^d , and A_2^n asymmetries are also presented for the purpose of comparison. The ability of determining the polarized sea-quark distributions are due to the impact of SIDIS data in which added to our data sample. The error bands, obtained through the Hessian method, are also shown as well. Upon examining the distributions in this figure, it becomes evident that the sea quark densities $x\delta\bar{u}$ and $x\delta\bar{d}$ exhibit relatively large uncertainties. Additionally, the input strange sea-quark distribution $x\delta s = x\delta\bar{s}$ displays the typical sign change.

Let us now discuss the results obtained by excluding the A_2 asymmetry measurements to examine the effect of these data sets on both the central values and extracted uncertainties. As observed in Fig. 4, the inclusion of the A_2 asymmetry data not only affects the central values of certain parton species but also impacts the error bands. These effects are most pronounced in the case of $x\delta\bar{u}$, $x\delta\bar{d}$, $x\delta s$, and gluon densities. The most significant changes are noticeable in the case of the gluon PDF in terms of central value, and in $x\delta\bar{d}$ and $x\delta s$ in terms of error bands. In terms of individual parton flavors, it can be observed that for $x\delta u + x\delta\bar{u}$ and $x\delta d + x\delta\bar{d}$, the two results exhibit a similar shape, with a slight reduction of error bands for $x\delta d + x\delta\bar{d}$. In the case of $x\delta\bar{u}$, when compared to the analysis excluding A_2 , it is evident that the distribution is slightly increased at large values of x and slightly decreased over the medium to small range of x , with the same size of error bands spanning the entire range of x . Regarding the xs density, in general, the shape remains nearly unchanged while the error band is increased. In the case of the gluon PDF, the inclusion of the A_2 asymmetry data significantly affects the central value, while the error band remains unchanged. Finally, for $x\delta\bar{d}$, the central values are the same, but the analysis including the A_2 asymmetry measurements leads to smaller error bands.

6.2 Comparison with other polrized PDFs

In this section, we present the AAK24 polarized PDFs and provide detailed comparisons with other results available in the literature, namely the results from DSSV14 [22], AKS14 [19], LSS10 [23], and JAM17 [24] all evaluated at the input

Table 5. The values of HT corrections extracted from the data in a model independent way.

x_i	$h^p(x_i) [\text{GeV}^2]$	x_i	$h^n(x_i) [\text{GeV}^2]$
0.028	0.03092 ± 0.00817	0.028	0.0418 ± 0.0170
0.100	-0.08545 ± 0.00386	0.100	0.0556 ± 0.0140
0.200	-0.04048 ± 0.00270	0.300	-0.01539 ± 0.0108
0.350	-0.03238 ± 0.00274	0.300	0.008924 ± 0.00581
0.600	-0.07021 ± 0.00443	0.500	-0.008407 ± 0.00374

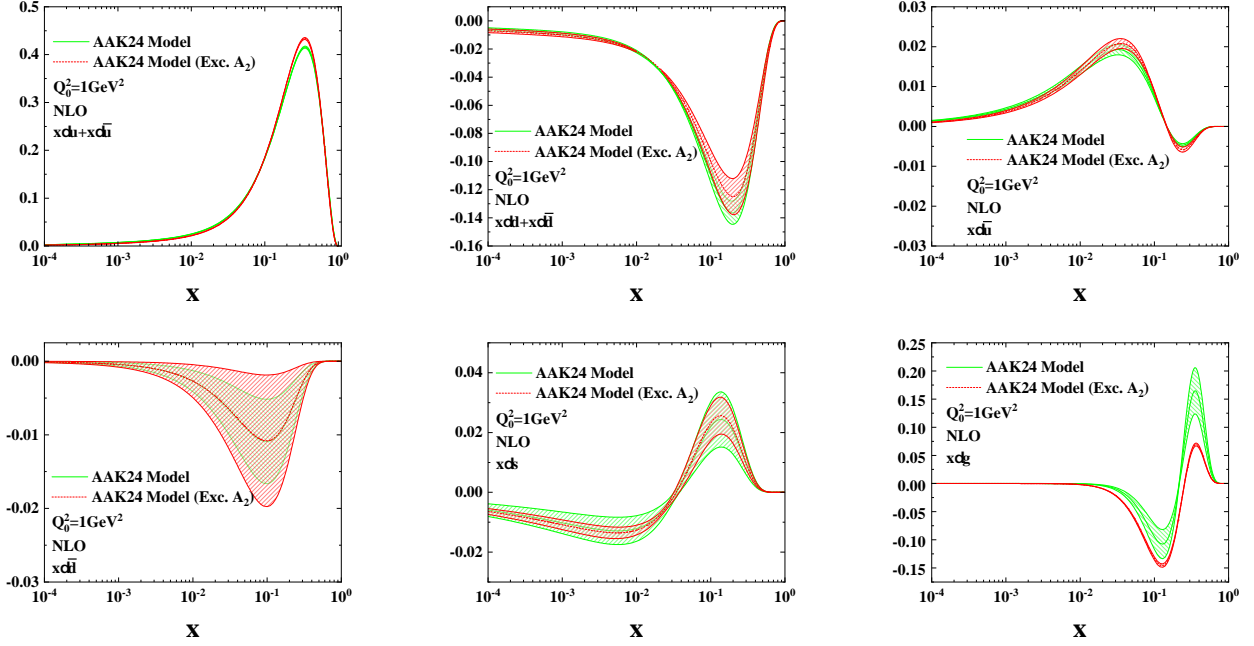


Fig. 4. The AAK24 quark and gluon helicity distributions at the input scale $Q_0^2 = 1 \text{ GeV}^2$ with and without the A_2 asymmetry measurements. The uncertainty bands, determined using the Hessian method, are also shown as well.

scale $Q_0^2 = 1 \text{ GeV}^2$ and at higher value of 10 GeV^2 . The comparisons are displayed in Figs. 5 and 6 at both the input scale of $Q^2 = 1 \text{ GeV}^2$ and a higher value of 10 GeV^2 .

Examining the $x\delta u + x\delta\bar{u}$ distribution, generally speaking, one can observe that all of the fits are in very good agreement with each other. In the case of the $\delta d + \delta\bar{d}$ distribution, all the groups agree very well, except for the DSSV14 result, which is smaller than those of the others at the input scale. However, the differences are within the uncertainty. As for $Q^2 = 10 \text{ GeV}^2$, the AAK24 polarized PDFs, JAM17 and LSS10 agree over the entire x region. However, for all other parton species, clear differences can be observed among the results of various groups.

A significant difference can be observed in the case of the sea-quark densities $x\delta\bar{u}$ and $x\delta\bar{d}$. For the case of $x\delta\bar{u}$, the AAK24 results are larger than those of other groups for $x < 0.1$ at the input scale. However, the difference becomes less pronounced at the higher scale. Despite the similar results between AAK24 and JAM17, for the $x\delta\bar{d}$ density at both input scale and higher values of $Q^2 = 10 \text{ GeV}^2$, the other results exhibit different behaviors at

Examining the strange distribution, we can observe that we obtained very similar results compared to those of JAM17 at the input scale. For the case of the gluon density $x\delta g$, the difference between all groups are more pronounced in this case. Like for the case of LSS10, our gluon density is smaller than those of others for medium value of x ; ($x \sim 0.1$)

Focusing on the JAM17 [24] polarized PDFs, one can observe significant differences in their gluon density $x\delta g$, $x\delta\bar{u}$, $x\delta\bar{d}$, and strange distribution compared to all other distributions presented in Fig. 5. Distinctions are also more apparent for $x\delta\bar{u}$ and $x\delta\bar{d}$, and $x\delta g$. It is essential to highlight that the AAK24 and JAM17 are very similar in the case of $x(\delta u + \delta\bar{u})$ and $x(\delta d + \delta\bar{d})$ and strange distribution.

These findings hold at a higher scale of 10 GeV^2 as well, as depicted in Fig. 6. Despite the similarity in $x(\delta u + \delta\bar{u})$ and $x(\delta d + \delta\bar{d})$, differences become more pronounced for the gluon density $x\delta g$, sea quarks and strange distribution $x\delta s$. It is crucial to emphasize that the JAM17 analysis employs the iterative Monte Carlo fitting technique, generating stable fits to polarized PDFs with statistically rigorous uncertainties.

6.3 The AAK24 fit quality and the data/theory comparison

We will now shift our focus to discussing the fit quality of AAK24 and conducting a detailed comparison of NLO theory predictions with the data analyzed in this study.

The quality of the AAK24 global QCD analysis is summarized in Tables. 1, 2 and 3. For both the A_1 and $\frac{g_1}{F_1}$ observables, we have presented both the total and individual χ^2 values in Table 1. It is noteworthy that in the total, we have considered 951 data points, resulting in a total χ^2 of 1170.172, which indicates a relatively good fit within

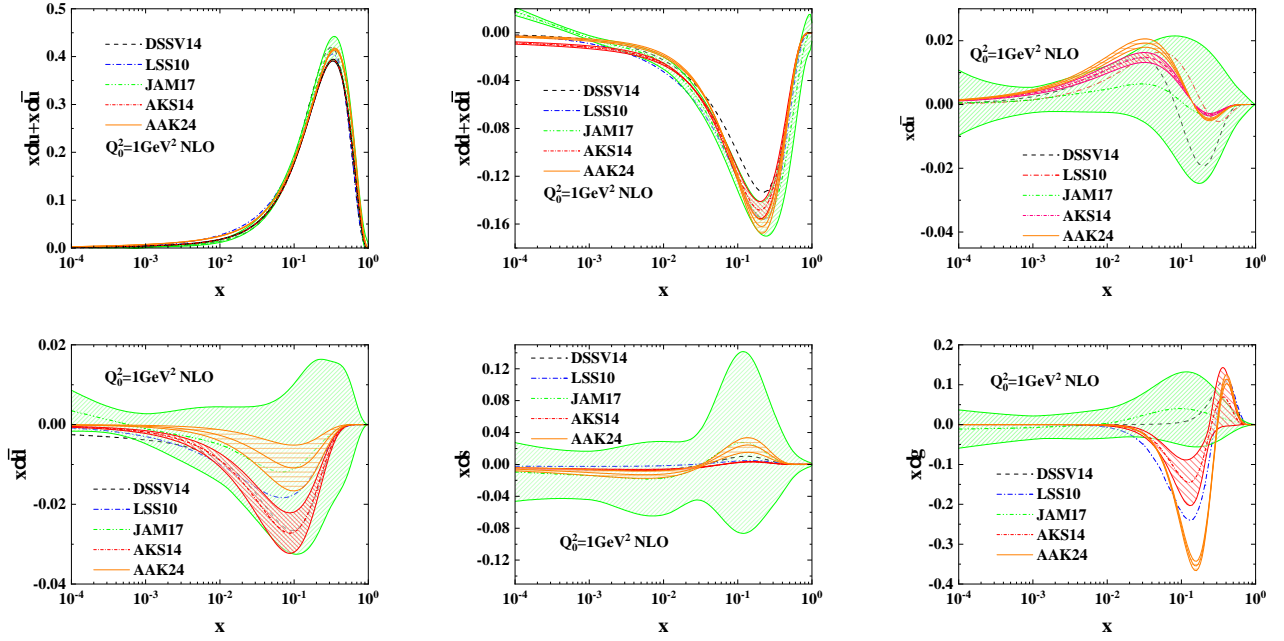


Fig. 5. The AAK24 quark and gluon helicity distributions at the input scale $Q_0^2 = 1 \text{ GeV}^2$, with uncertainty bands now clearly corresponding to the different PDF sets. The comparisons include DSSV14 [22] (black dashed), LSS10 [23] (blue dashed dotted), JAM17 [24] (green dashed dot dotted), and AKS14 [19] (red short dashed dotted). The uncertainty bands for each set are shown with the same color as their corresponding line in the legend.

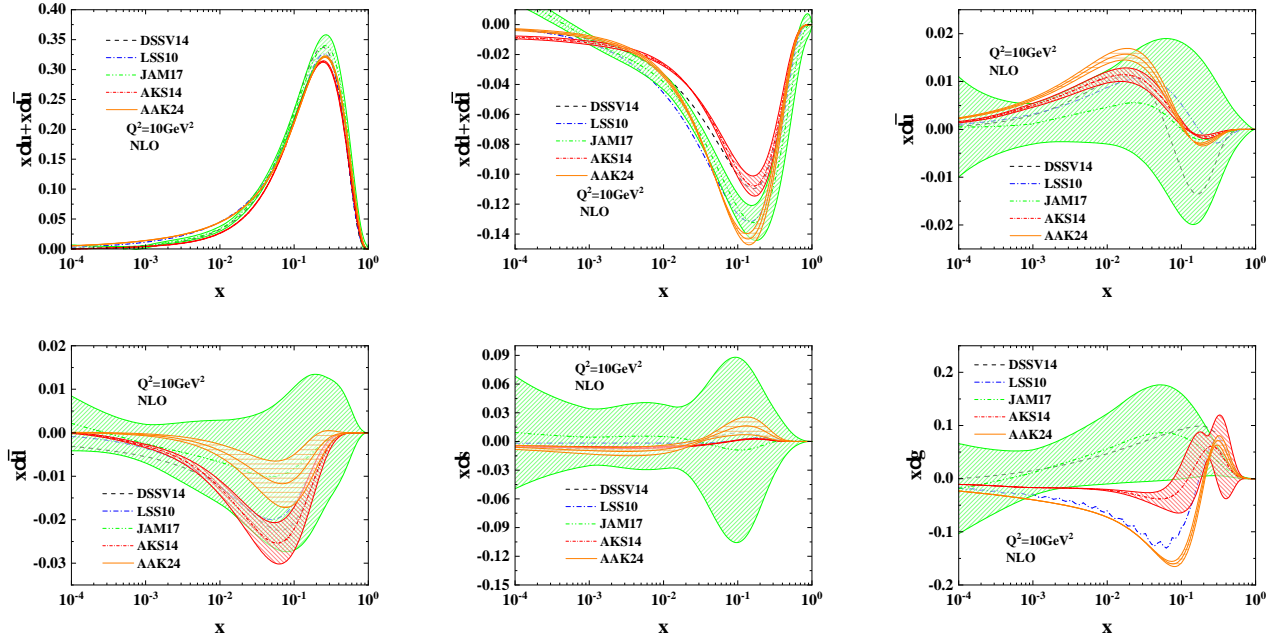


Fig. 6. Same as Fig. 5 but this time at the higher value of 10 GeV^2 .

the framework of QCD. When examining individual χ^2 values, it becomes evident that in most cases, there is a strong agreement between the data and theory. This is particularly evident in the case of the CLAS data, which contributes significantly to the total dataset with 136 data points for A_1^p and 452 for A_1^d . For the newly added COMPASS and JLAB data, our observations indicate that the fit quality is generally good for COMPASS16 and COMPASS17. However, for the JLAB17 dataset, a less favorable χ^2 value is obtained, suggesting a relatively worse agreement between the data and theoretical predictions in this case.

The corresponding χ^2 for the A_2 asymmetry observables, with a total of $N_{dat} = 140$ data points, are available in Table. 2. It is worth noting that not only do we achieve a very favorable total χ^2 value, but we also observe good individual χ^2 values for datasets originating from various experiments analyzed in this work. This suggests a strong agreement between the data and theoretical predictions across different experimental sources.

Finally, Table. 3 provides the χ^2 values for the A_{1N}^h SIDIS observables that have been examined in this study as well, encompassing a total of $N_{dat} = 160$ data points. As is evident from this table, the individual χ^2 values for each experiment exhibit a consistent and stable pattern, and the overall total values indicate a good agreement between the data and the theoretical predictions.

As discussed earlier, an additional analysis was performed where the A_2 asymmetry observables (data in Table. 2) were excluded from the QCD fit. The corresponding χ^2 values per data point are presented in the last column of Tables. 1 and 3. The numbers in these tables suggest that the exclusion of A_2 asymmetry data could potentially increase the total values of χ^2 . Table. 1 shows that the inclusion of A_2 data increases the total value of χ^2 from 1170.172 to 1304.509. Similarly, Table. 3 indicates an increase in the total value of χ^2 from 227.934 to 244.520.

In summary, the global χ^2/N_{dat} value for the entire dataset of 1266 data points in the AAK24 global QCD analysis is calculated to be 1.0528. This value indicates a stable and acceptable fit quality, demonstrating that the theoretical model aligns well with the experimental data. However, when the A_2 asymmetry observables are excluded, the χ^2/N_{dat} value increases to 1.0647. This result underscores the significance of including the A_2 asymmetry data in QCD analyses of polarized PDFs. It suggests that the inclusion of A_2 data leads to a better-constrained set of polarized PDFs with improved agreement between the data and theory, emphasizing the importance of these measurements in refining our understanding of polarized PDFs.

We can now proceed to compare the NLO theory predictions obtained for the asymmetry observables used in this study with the experimental datasets, particularly the newly added polarized data from COMPASS16 [6] and COMPASS17 [27] experiments, focusing on the A_1^p and A_1^d asymmetries. Such comparisons are displayed in Figs. 7 and 8 for the A_1^p and A_1^d asymmetry data from the COMPASS16 and COMPASS17 experiments, respectively. The comparisons are made as functions of x for two different selections of Q^2 , specifically 15 and 13 GeV². As these plots illustrate, the predictions from the AAK24 polarized PDFs are in excellent agreement with both the COMPASS16 and COMPASS17 datasets across the entire range of x . These results align with the individual χ^2 values presented in Table. 1, further confirming the quality of the fit and the compatibility between the theoretical model and the experimental data.

In Figs. 9 and 10, we present the polarized proton structure functions xg_2^p calculated using the Wandzura-Wilczek relation in Eq. 6. The results from NMA23 (dashed dashed dotted) [21] and KTA17 (dashed dotted) [20] are also shown. The experimental data from the E155 collaboration [59] are included for comparison. As can be seen, the xg_2^p structure functions calculated using the Wandzura-Wilczek approximation provide good agreement with both the data and other results available in the literature.

To provide additional support for our discussion regarding the comparison between data and theory, we present detailed comparisons of our theoretical predictions with a different selection of A_1^p asymmetry data as outlined in Table. 1. As one can see from Fig. 11, the agreement between the theoretical model and various selections of A_1^p asymmetry data is good. Such agreement between the theoretical predictions and a variety of experimental datasets for A_1^p asymmetry provides evidence of the validity and reliability of the AAK24 analysis in describing the polarized PDFs in nucleons.

We are now in a position to compare the theoretical predictions from AAK24 with the corresponding experimental results for the SIDIS asymmetries. This comparison is illustrated in Fig. 12 for selected data from SMC and COMPASS collaborations. Our calculations include the theory predictions for proton, neutron, and deuteron, taking into account the light charged hadron, kaon, and pion FFs. As shown in the figures, the agreement between the data and theory is excellent across the entire range of x and for all hadron species. This alignment corroborates the favorable χ^2 values presented in Table. 3. It further confirms the consistency between the theoretical framework and the experimental data, affirming the model ability to accurately describe the observed phenomena in the realm of polarized SIDIS asymmetries.

To provide more detailed discussions of the results, we provide a comparison in Fig. 13 between the AAK24 theoretical predictions for the A_2 asymmetry for proton, neutron, and deuteron targets and the corresponding data analyzed in this study. As mentioned earlier, this marks the first inclusion of A_2 asymmetry data in a global QCD analysis of polarized PDFs. Upon inspection, the data/theory agreement is generally good for most experiments. However, some deviations between the data and theory are evident. For example, discrepancies can be observed for the A_2^d asymmetry from the SMC experiment and the A_2^p asymmetry from HERMES.

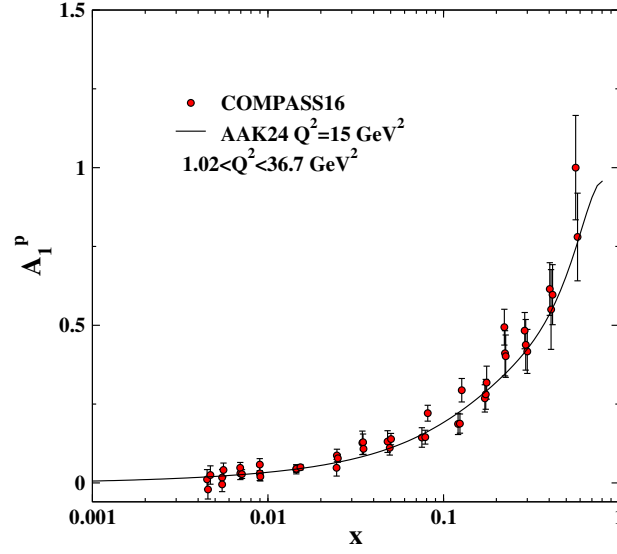


Fig. 7. Comparison of the AAK24 theory prediction with the A_1^p asymmetry data from COMPASS16 experiment [6].

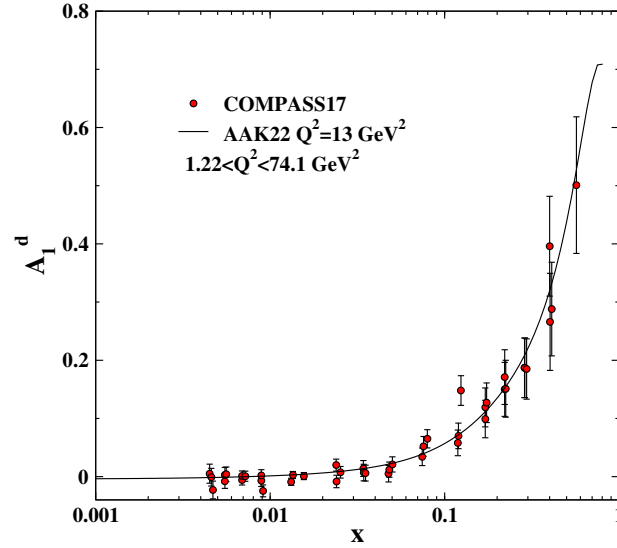


Fig. 8. Same as Fig. 7 but this time for the A_1^d asymmetry data from COMPASS17 experiment [27].

In summary, the AAK24 results presented in this section, which integrated recent experimental data from JLAB17, COMPASS16, and COMPASS17, including the novel inclusion of A_2 asymmetry measurements, exhibited favorable overall agreement with experimental data. These findings also align well with other polarized PDF determinations, notably JAM17, DSSV14, LSS10, and AKS14, all of which also accounted for SU(2) and SU(3) symmetry breaking.

7 Conclusions

In this article, we have presented AAK24 polarized PDFs, a next-to-leading order (NLO) QCD analysis of polarized data from both polarize DIS and SIDIS experiments on the nucleon. Throughout the analysis, we considered the scenario of SU(2) and SU(3) symmetry breaking, specifically $\delta\bar{u} \neq \delta\bar{d} \neq \delta\bar{s}$, while treating $\delta\bar{s}$ and δs as equal since the available experimental data are not enough to distinguish them. Additionally, we have included the nonperturbative target mass corrections (TMC) as well as higher-twist terms (HT) which are particularly important for the polarized DIS. Our study addressed the crucial role of semi-inclusive data in determining the polarized sea quark distributions. The recent experimental data from JLAB17, COMPASS16, and COMPASS17 experiments have been incorporated into our

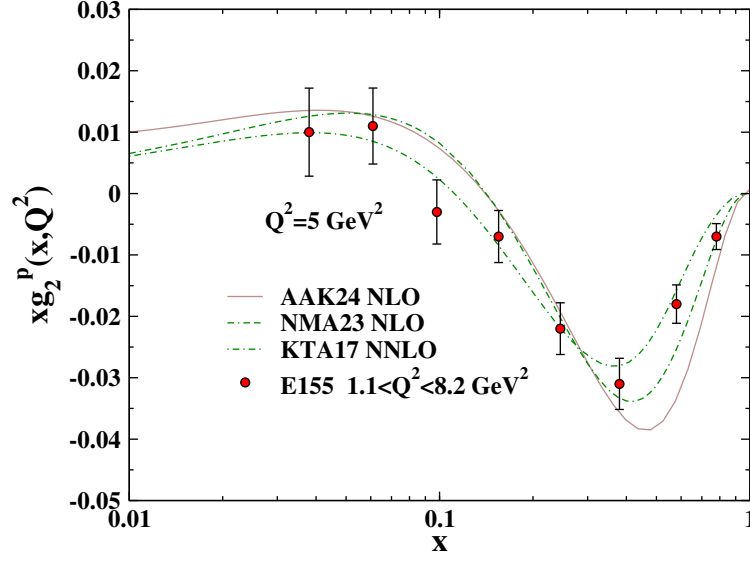


Fig. 9. The polarized proton structure functions xg_2^p as a function of x at $Q^2 = 5 \text{ GeV}^2$. The results from NMA23 (dashed dashed dotted) [21] and KTA17 (dashed dotted) [20] are also shown. The experimental data from the E155 collaboration [59] are presented for comparison.

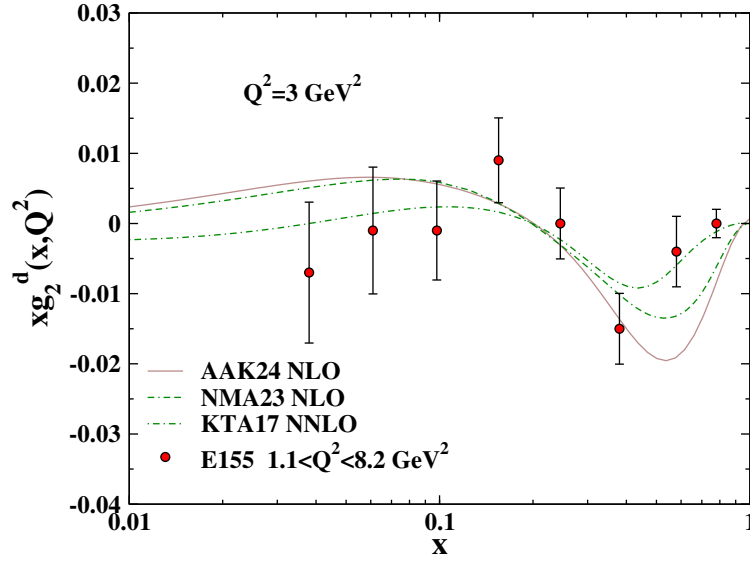


Fig. 10. Same as Fig. 9, but this time the comparisons are shown for $Q^2 = 3 \text{ GeV}^2$.

data samples. Additionally, this analysis marks simultaneous incorporation of SIDIS and A_2 asymmetry measurements as well.

We have thoroughly examined the impact of these new data sets on both the central values and the extracted uncertainties, as well as their effect on the overall fit quality. Our findings are presented and discussed to provide a comprehensive understanding of their implications. To quantify the uncertainties in the polarized PDFs, we employed the standard Hessian method. The main results of AAK24 QCD analysis exhibit an overall good agreement with the analyzed experimental data, aligning well with other polarized PDFs determinations which considered the SU(2) and SU(3) symmetry breaking as well.

A Fortran package containing AAK24 polarized PDFs at NLO accuracy can be obtained via e-mail from the authors.

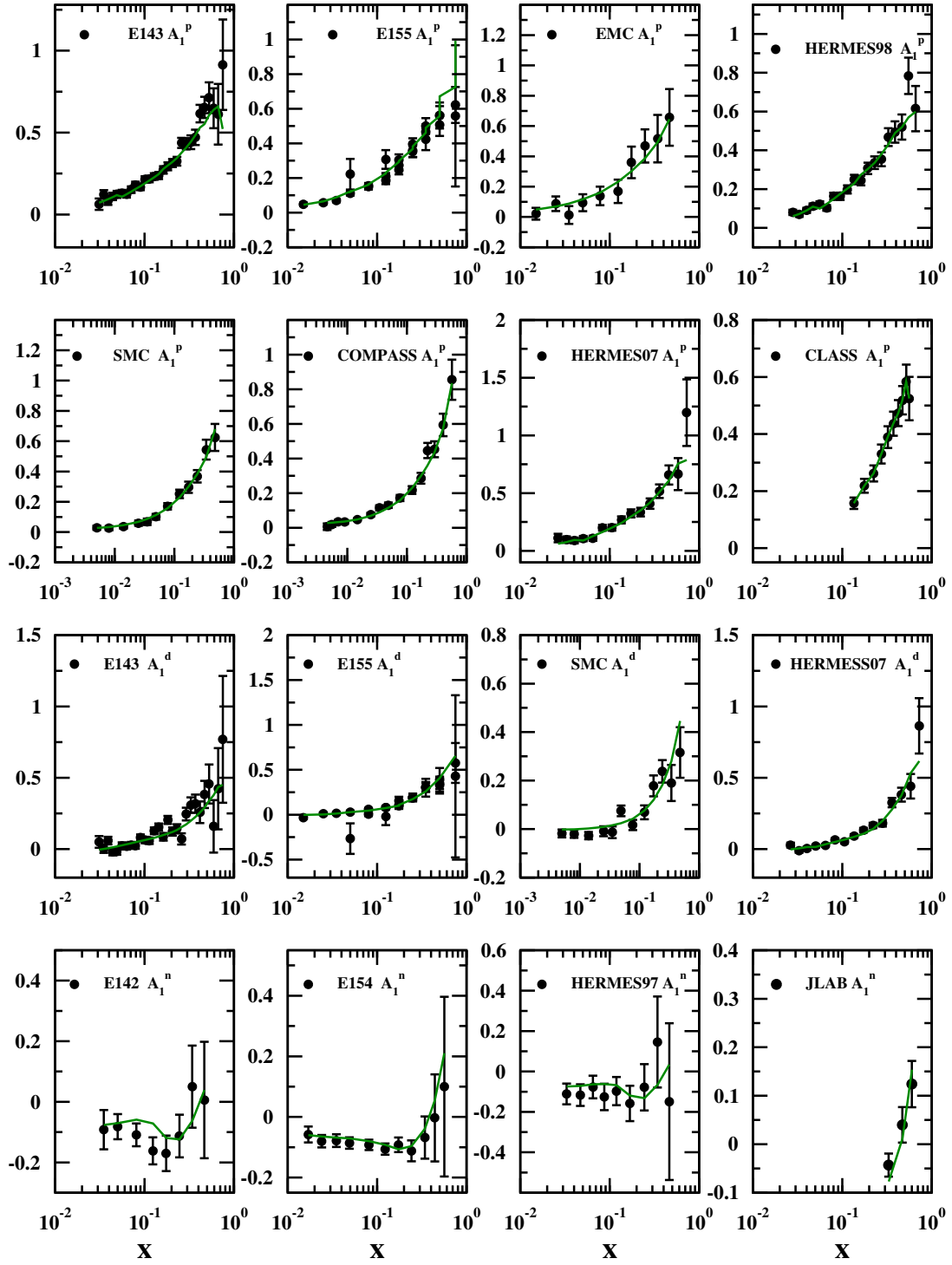


Fig. 11. Comparison of the AAK24 theory prediction with some selection of A_1^p , A_1^n , and A_1^d asymmetry data presented in Table. 1.

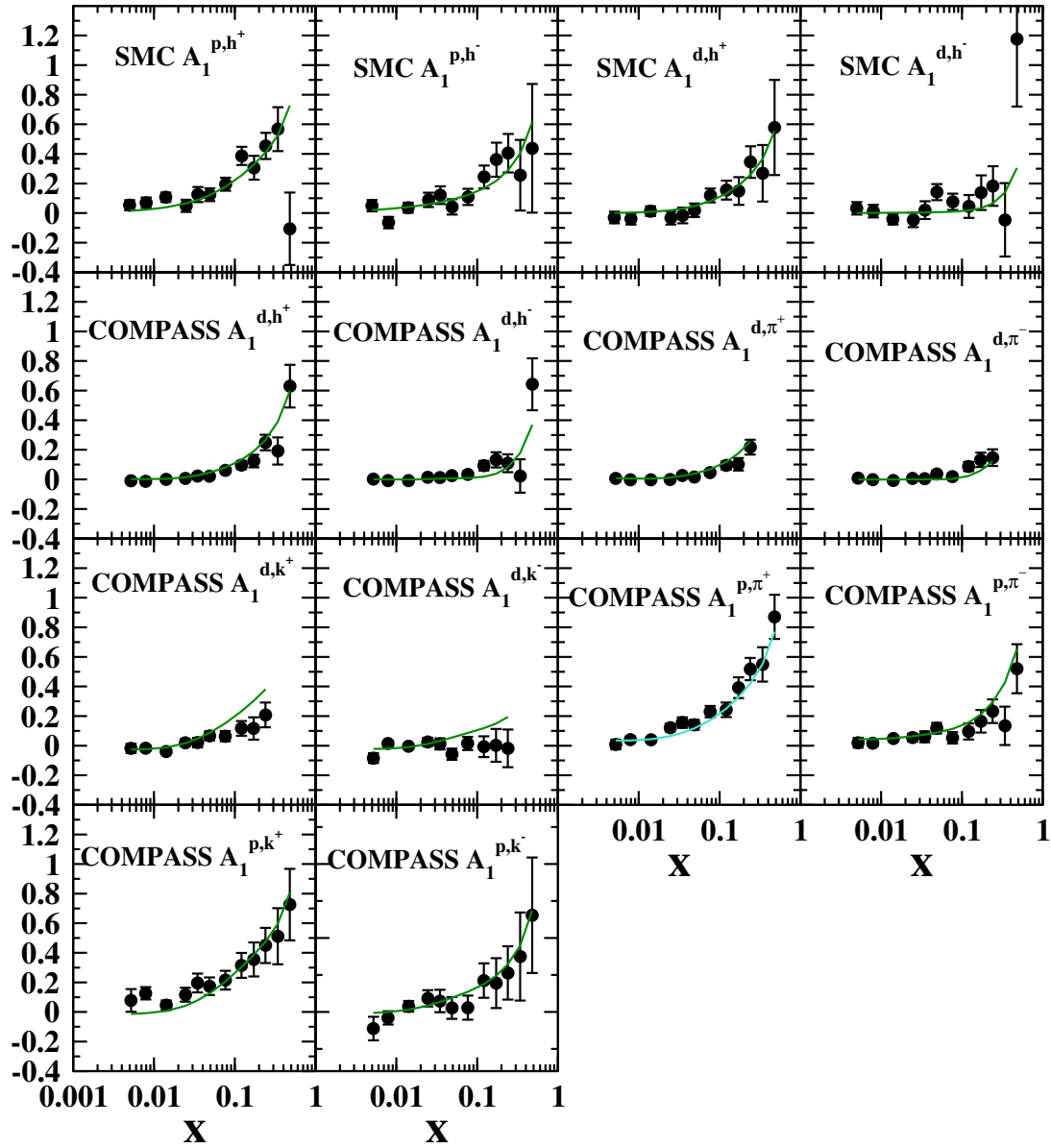


Fig. 12. Comparison of AAK24 QCD results for the SIDIS asymmetries with the corresponding SIDIS observables. The calculations include the theory predictions for proton, neutron, and deuteron, taking into account the light charged hadron, kaon, and pion FFs.

Data Availability Statement

This manuscript has associated data in a data in a repository. [Authors comment: This data sets generated during the current study are available from the corresponding author on responsible request.]

Acknowledgments

The authors appreciate the financial support from the Iran National Science Foundation (INSF) under grant number 4013570. S. A. T. and H. K. are also grateful to the School of Particles and Accelerators, Institute for Research in Fundamental Sciences (IPM). F. A. acknowledges the Farhangian University for the provided support to conduct this research. H. Khanpour appreciates the financial support from NAWA under grant number BPN/UML/2023/1/00160 and from the IDUB programme at the AGH University. We also thank Dimitar Stamenov for providing the necessary LSS10 grids, and Rodolfo Sassot for supplying the required DSSV14 grids data.

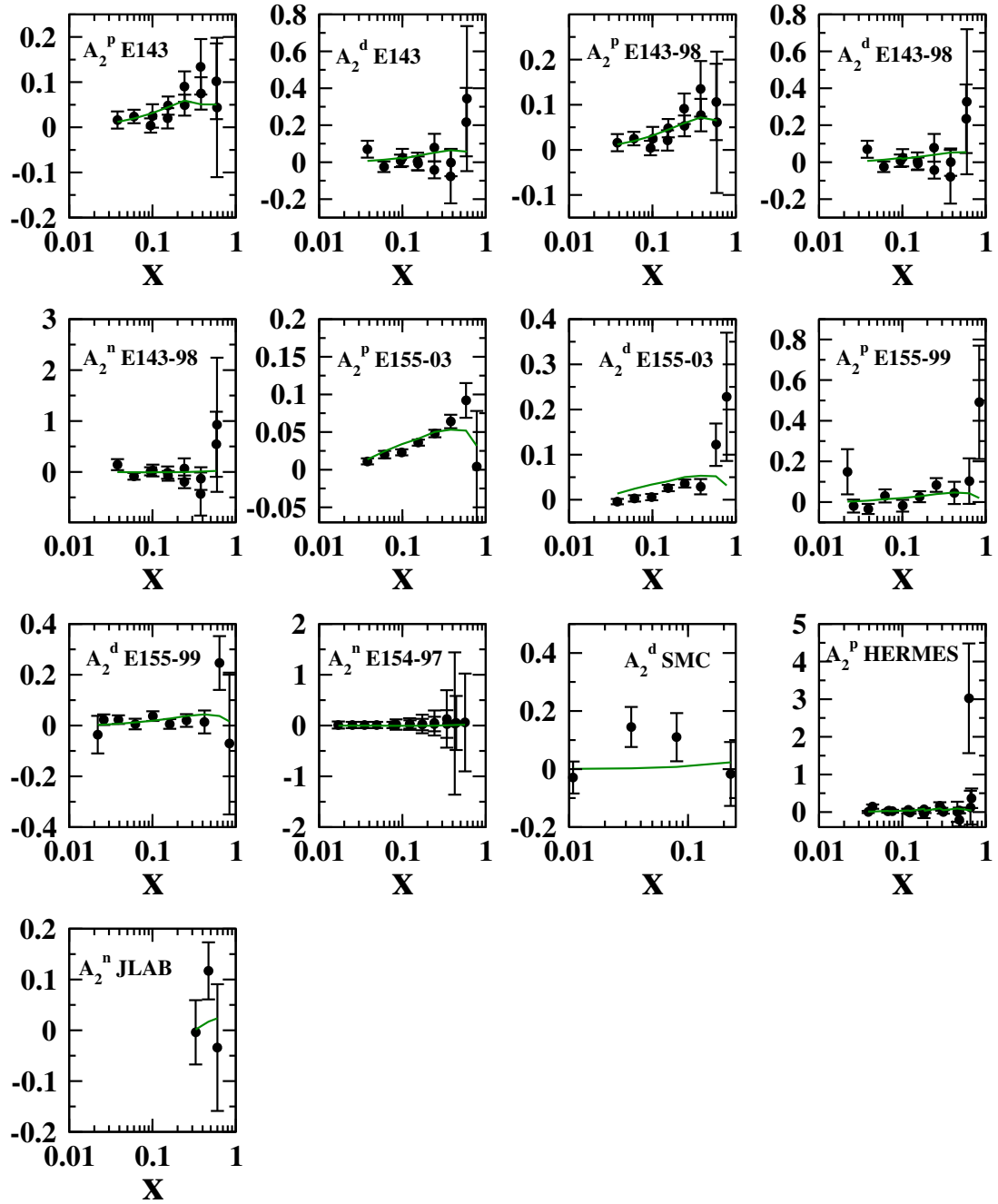


Fig. 13. Comparison of AAK24 QCD results for the A_2 asymmetries with a selected set of corresponding data. The calculations include the theory predictions for proton, neutron, and deuteron

References

1. A. Deur, S. J. Brodsky and G. F. De Téramond, Rept.Prog.Phys. 82 (2019) 076201
2. C. A. Aidala, S. D. Bass, D. Hasch and G. K. Mallot, Rev. Mod. Phys. **85**, 655-691 (2013),
3. J. J. Ethier and E. R. Nocera, Ann. Rev. Nucl. Part. Sci. **70**, 43-76 (2020)
4. R. Abdul Khalek, A. Accardi, J. Adam, D. Adamiak, W. Akers, M. Albaladejo, A. Al-bataineh, M. G. Alexeev, F. Ameli and P. Antonioli, *et al.* Nucl. Phys. A **1026**, 122447 (2022),
5. D. P. Anderle, T. J. Hou, H. Xing, M. Yan, C. P. Yuan and Y. Zhao, JHEP **08**, 034 (2021),
6. C. Adolph *et al.* [COMPASS], Phys. Lett. B **753**, 18-28 (2016)
7. D. De Florian, G. A. Lucero, R. Sassot, M. Stratmann and W. Vogelsang, Phys. Rev. D **100**, no.11, 114027 (2019)
8. T. Khan, T. Liu and R. S. Sufian, Phys. Rev. D **108**, no.7, 074502 (2023)
9. D. Adamiak *et al.* [Jefferson Lab Angular Momentum], Phys. Rev. D **104**, no.3, L031501 (2021)
10. F. Arbabifar, S. Atashbar Tehrani and H. Khanpour, Phys. Rev. C **108**, no.3, 035203 (2023)
11. F. Taghavi-Shahri, H. Khanpour, S. Atashbar Tehrani and Z. Alizadeh Yazdi, Phys. Rev. D **93**, no.11, 114024 (2016)
12. M. Hirai *et al.* [Asymmetry Analysis], Nucl. Phys. B **813**, 106-122 (2009)
13. E. Leader, A. V. Sidorov and D. B. Stamenov, Phys. Rev. D **91**, no.5, 054017 (2015)
14. H. Khanpour, S. T. Monfared and S. Atashbar Tehrani, Phys. Rev. D **95**, no.7, 074006 (2017),
15. N. Sato *et al.* [Jefferson Lab Angular Momentum], Phys. Rev. D **93**, no.7, 074005 (2016),
16. J. Blumlein and H. Bottcher, Nucl. Phys. B **841** (2010) 205
17. D. de Florian, R. Sassot, M. Stratmann and W. Vogelsang, Phys. Rev. D **80** (2009) 034030
18. D. Adamiak, N. Baldonado, Y. V. Kovchegov, W. Melnitchouk, D. Pitonyak, N. Sato, M. D. Sievert, A. Tarasov and Y. Tawabutr, [arXiv:2308.07461 [hep-ph]].
19. F. Arbabifar, A. N. Khorramian and M. Soleymaninia, Phys. Rev. D **89**, no.3, 034006 (2014)
20. H. Khanpour, S. T. Monfared and S. Atashbar Tehrani, Phys. Rev. D **95**, no.7, 074006 (2017)
21. H. Nematollahi, A. Mirjalili and S. Atashbar Tehrani, Phys. Rev. D **107**, no.5, 054033 (2023)
22. D. de Florian, R. Sassot, M. Stratmann and W. Vogelsang, Phys. Rev. Lett. **113**, no.1, 012001 (2014)
23. E. Leader, A. V. Sidorov and D. B. Stamenov, Phys. Rev. D **82**, 114018 (2010)
24. N. Sato *et al.* [Jefferson Lab Angular Momentum], Phys. Rev. D **93**, no.7, 074005 (2016)
25. C. Amsler *et al.* (Particle Data Group), Phys. Lett. B **667** (2008) 1.
26. H. J. Lipkin, Phys. Lett. B **214**, 429 (1988); Phys. Lett. B **230**, 135 (1989); F. E. Close and R. G. Roberts, Phys. Rev. Lett. **60**, 1471 (1988); M. Roos, Phys. Lett. B **246**, 179 (1990); Z. Dziembowski and J. Franklin, J. Phys. G **17**, 213 (1991). P. G. Ratcliffe, Phys. Lett. B **242**, 271 (1990); Phys. Lett. B **365**, 383 (1996); arXiv:hep-ph/0012133; S. L. Zhu, G. Sacco, and M. J. Ramsey-Musolf, Phys. Rev. D **66**, 034021 (2002); E. Leader and D. B. Stamenov, Phys. Rev. D **67**, 037503 (2003).
27. C. Adolph *et al.* [COMPASS], Phys. Lett. B **769**, 34-41 (2017)
28. R. Fersch *et al.* [CLAS], Phys. Rev. C **96**, no.6, 065208 (2017)
29. B. Lampe and E. Reya, Phys. Rept. **332**, 1-163 (2000),
30. Y. B. Dong, Phys. Lett. B **641**, 272 (2006).
31. Y. B. Dong, Phys. Rev. C **78**, 028201 (2008)
32. Y. B. Dong, Phys. Lett. B **653**, 18 (2007)
33. Y. B. Dong and D. Y. Chen, Nucl. Phys. A **791**, 342 (2007).
34. A. V. Sidorov and D. B. Stamenov, Mod. Phys. Lett. A **21**, 1991 (2006)
35. O. Nachtmann, Nucl. Phys. B **63**, 237 (1973).
36. A. Piccione and G. Ridolfi, Nucl. Phys. B **513**, 301-316 (1998)
37. A. Courtoy, A. S. Miramontes, H. Avakian, M. Mirazita and S. Pisano, Phys. Rev. D **106**, no.1, 014027 (2022),
38. A. Mirjalili and S. Atashbar Tehrani, Phys. Rev. D **105**, no.7, 074023 (2022)
39. L. W. Whitlow, S. Rock, A. Bodek, E. M. Riordan and S. Dasu, Phys. Lett. B **250**, 193-198 (1990)
40. M. Arneodo *et al.* [New Muon], Phys. Lett. B **364**, 107-115 (1995)
41. D. de Florian, M. Stratmann and W. Vogelsang, Phys. Rev. D **57**, 5811-5824 (1998),
42. A. D. Martin, R. G. Roberts, W. J. Stirling and R. S. Thorne, Eur. Phys. J. C **28**, 455-473 (2003)
43. T. J. Hou, J. Gao, T. J. Hobbs, K. Xie, S. Dulat, M. Guzzi, J. Huston, P. Nadolsky, J. Pumplin and C. Schmidt, *et al.* Phys. Rev. D **103**, no.1, 014013 (2021)
44. D. de Florian, R. Sassot, and M. Stratmann, Phys. Rev. D **75**, 114010 (2007) Phys. Rev. D **76**, 074033 (2007)
45. J. Ashman *et al.* [European Muon Collaboration], J. Ashman *et al.* [European Muon Collaboration], Nucl. Phys. B **328** (1989) 1.
46. B. Adeva *et al.* [Spin Muon Collaboration], Phys. Rev. D **58** (1998) 112001.
47. M. G. Alekseev *et al.* [COMPASS Collaboration], Phys. Lett. B **690**, 466 (2010) V. Y. Alexakhin *et al.* [COMPASS Collaboration], Phys. Lett. B **647** (2007) 8
48. P. L. Anthony *et al.* [E142 Collaboration], Phys. Rev. D **54** (1996) 6620
49. K. Abe *et al.* [E143 collaboration], Phys. Rev. D **58** (1998) 112003
50. K. Abe *et al.* [E154 Collaboration], Phys. Rev. Lett. **79** (1997) 26
51. P. L. Anthony *et al.* [E155 Collaboration], Phys. Lett. B **493** (2000) 19
52. P. L. Anthony *et al.* [E155 Collaboration], Phys. Lett. B **463** (1999) 339

53. SMC Collaboration, B. Adeva *et al.*, Phys. Lett. B **420** (1998) 180.
54. K. Ackerstaff *et al.* [HERMES Collaboration], Phys. Lett. B **404** (1997) 383 A. Airapetian *et al.* [HERMES Collaboration], Phys. Lett. B **442** (1998) 484
55. A. Airapetian *et al.* [HERMES Collaboration], Phys. Rev. D **75** (2007) 012007
56. K. V. Dharmawardane *et al.* [CLAS Collaboration], Phys. Lett. B **641** (2006) 11
57. X. Zheng *et al.* (JLab/Hall A Collaboration), Phys. Rev. Lett. **92**, 012004 (2004);
58. K. Abe *et al.* [E143], Phys. Rev. Lett. **76**, 587-591 (1996)
59. P. L. Anthony *et al.* [E155], Phys. Lett. B **553**, 18-24 (2003)
60. P. L. Anthony *et al.* [E155], Phys. Lett. B **458**, 529-535 (1999)
61. K. Abe *et al.* [E154], Phys. Lett. B **404**, 377-382 (1997)
62. D. Adams *et al.* [Spin Muon (SMC)], Phys. Lett. B **396**, 338-348 (1997)
63. A. Airapetian *et al.* [HERMES], Eur. Phys. J. C **72**, 1921 (2012)
64. M.G. Alekseev *et al.* (COMPASS Collaboration), Phys. Lett. B **660**, 458 (2008).
65. M.G. Alekseev *et al.* (COMPASS Collaboration), Phys. Lett. B **680**, 217 (2009).
66. M. G. Alekseev *et al.* [COMPASS Collaboration], Phys. Lett. B **693** (2010) 227
67. F. James and M. Roos, Comput. Phys. Commun. **10**, 343 (1975); F. James, "MINUIT Function Minimization and Error Analysis: Reference Manual Version 94.1," CERN-D-506, CERN-D506.
68. J. Pumplin, D. Stump, R. Brock, D. Casey, J. Huston, J. Kalk, H. L. Lai and W. K. Tung, Phys. Rev. D **65**, 014013 (2001),
69. A. Accardi, T. J. Hobbs, X. Jing and P. M. Nadolsky, Eur. Phys. J. C **81**, no.7, 603 (2021),